

before the cap carbonate precipitated. This may explain the lack of a sharp Ir spike at the base of the Sturtian cap carbonate. Alternatively, during the Sturtian glacial epoch, Earth's surface may not have been fully covered with ice on which extraterrestrial material could accumulate for a long time; however, the presence of banded iron formations in and below Sturtian glacials suggests that the ocean was ice-covered at that time (3).

# References and Notes

1. J. L. Kirschvink, in *The Proterozoic Biosphere*, J. W. Schopf, C. Klein, Eds. (Cambridge Univ. Press, Cambridge, 1992), pp. 51–52.
2. P. F. Hoffman, A. J. Kaufman, G. P. Halverson, D. P. Schrag, *Science* **281**, 1342 (1998).
3. P. E. Hoffman, D. P. Schrag, *Terra Nova* **14**, 129 (2002).
4. W. T. Hyde, T. J. Crowley, S. K. Baum, W. R. Peltier, *Nature* **405**, 425 (2000).
5. T. J. Crowley, W. T. Hyde, W. R. Peltier, *Geophys. Res. Lett.* **28**, 283 (2001).
6. K. Caldeira, J. F. Kasting, *Nature* **359**, 226 (1992).

7. K. Caldeira, *Geology* **19**, 204 (1991).
8. L. E. Sohl, N. Christie-Blick, D. V. Kent, *Geol. Soc. Am. Bull.* **111**, 1120 (1999).
9. Materials and methods are available as supporting material on Science Online.
10. C. Koeberl, H. Huber, *J. Radioanal. Nucl. Chem.* **244**, 655 (2000).
11. J. T. Wasson, in *Meteorites: Their Record of Solar System History* (Freeman, New York, 1985), p. 267.
12. Z. Cepelch, *Astron. Astrophys.* **263**, 361 (1992).
13. K. A. Parley, D. B. Patterson, *Nature* **378**, 600 (1995).
14. F. T. Kyte, J. T. Wasson, *Science* **232**, 1225 (1986).
15. E. Anders, N. Grevesse, *Geochim. Cosmochim. Acta* **53**, 197 (1989).
16. H. Heinrich, *Quat. Res.* **29**, 142 (1988).
17. J. D. Roberts, *J. Geol.* **84**, 47 (1974).
18. I. J. Fairchild, in *Sedimentology Review*, V. P. Wright, Ed. (Blackwell, Oxford, 1993), pp. 1–16.
19. M. J. Kennedy, *J. Sediment. Res.* **66**, 1050 (1996).
20. D. C. Noble, W. L. Rigot, H. R. Bowman, *GSA Spec. Pap.* **180**, 77 (1979).
21. Basaltic Volcanism Study Project, in *Basaltic Volcanism on the Terrestrial Planets* (Pergamon, New York, 1981), p. 1286.
22. B. Peucker-Ehrenbrink, *Geochim. Cosmochim. Acta* **60**, 3192 (1996).
23. F. Marcantonio et al., *Nature* **383**, 705 (1996).

24. F. Marcantonio et al., *Geochim. Cosmochim. Acta* **62**, 1535 (1998).
25. F. Marcantonio et al., *Earth Planet. Sci. Lett.* **170**, 157 (1999).
26. B. Schmitz, B. Peucker-Ehrenbrink, M. Lindström, M. Tassinari, *Science* **278**, 88 (1997).
27. A. H. Knoll, M. R. Walter, *Nature* **356**, 673 (1992).
28. J. P. Grotzinger, S. A. Bowring, B. Z. Saylor, A. J. Kaufman, *Science* **270**, 598 (1995).
29. H. Porada, *Precambrian Res.* **44**, 103 (1989).
30. R. M. Key et al., *J. Afr. Earth Sci.* **33**, 503 (2001).
31. We thank H. Rice and F. Popp from the University of Vienna for discussions and comments. This work was supported by the Austrian Science Foundation. This is University of the Witwatersrand Impact Cratering Research Group publication no. 93.

# Supporting Online Material

www.sciencemag.org/cgi/content/full/308/5719/239/DC1

Materials and Methods

Fig. S1

Tables S1 to S3

References and Notes

30 August 2004; accepted 18 January 2005  
10.1126/science.1104657

## The Brain of LB1, *Homo floresiensis*

Dean Falk,<sup>1\*</sup> Charles Hildebolt,<sup>2</sup> Kirk Smith,<sup>2</sup> M. J. Morwood,<sup>3</sup> Thomas Sutikna,<sup>4</sup> Peter Brown,<sup>3</sup> Jatmiko,<sup>4</sup> E. Wayhu Saptomo,<sup>4</sup> Barry Brunnsden,<sup>2</sup> Fred Prior<sup>2</sup>

The brain of *Homo floresiensis* was assessed by comparing a virtual endocast from the type specimen (LB1) with endocasts from great apes, *Homo erectus*, *Homo sapiens*, a human pygmy, a human microcephalic, specimen number Sts 5 (*Australopithecus africanus*), and specimen number WT 17000 (*Paranthropus aethiopicus*). Morphometric, allometric, and shape data indicate that LB1 is not a microcephalic or pygmy. LB1's brain/body size ratio scales like that of an australopithecine, but its endocast shape resembles that of *Homo erectus*. LB1 has derived frontal and temporal lobes and a lunate sulcus in a derived position, which are consistent with capabilities for higher cognitive processing.

The type specimen of *Homo floresiensis* (LB1, female) (1) has a brain size of ~400 cm<sup>3</sup>, which is similar to that of *Australopithecus afarensis* specimen AL 288-1 (Lucy) (2), who lived approximately 3.0 million years ago. Yet LB1's species was associated with big-game stone technology, remains of *Stegodon*, and charred animal bones that hint at the use of fire and cooking. Its ancestors also had to cross the sea to reach the Indonesian island of Flores (3). Could a tiny hominin with an ape-sized brain really have engaged in such advanced behaviors? Some workers reject the notion that LB1

represents a new species that was closely tied to *H. erectus* (1) and suggest instead that it was a pathological human microcephalic (4). To help address this debate, we compared three-dimensional computed tomographic (3DCT) reconstructions of the internal braincase (virtual endocasts) that reproduce details of external brain morphology, including sulci, vessels, sinuses, cranial capacity, and shape (5–8), from LB1, an adult female chimpanzee, an adult female *H. erectus* (specimen ZKD XI), a contemporary woman, and a European microcephalic. To broaden taxonomic comparisons and supplement limited sample size, our analysis also included endocasts of the skulls of specimen Sts 5 (*A. africanus*), specimen KNM-WT 17000 (*Paranthropus aethiopicus*), 10 humans, 10 gorillas, 18 chimpanzees (9), an adult female pygmy, and five *H. erectus*.

Our virtual cranial capacity estimate for LB1 is 417 cm<sup>3</sup> (10). Virtual endocasts of the microcephalic, modern woman, *H. erectus*, and chimpanzee were scaled to 417 cm<sup>3</sup> to facili-

tate shape comparisons (Fig. 1 and fig. S2). LB1's shape most resembles that of ZKD XI, which is typical of classic *H. erectus* from China and Java (Trinil) (fig. S3). Both endocasts are noticeably wider caudally than rostrally (Fig. 1A), wider ventrally than dorsally (fig. S2), and relatively long and low in lateral profile (Fig. 1B). However, LB1 lacks the de-

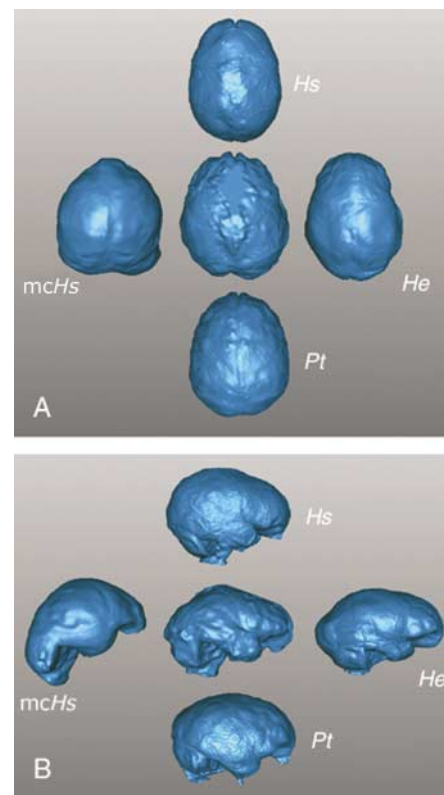


**Fig. 1.** Comparisons of virtual endocasts of LB1 (center). (A) Dorsal views. (B) Right lateral views. Hs, *H. sapiens*; Pt, *Pan troglodytes*; mChs, a human microcephalic; He, *H. erectus*.

<sup>1</sup>Department of Anthropology, Florida State University, Tallahassee, FL 32306, USA. <sup>2</sup>Mallinckrodt Institute of Radiology, Washington University School of Medicine, St. Louis, MO 63110, USA. <sup>3</sup>Archaeology and Palaeoanthropology, University of New England, Armidale, New South Wales 2351, Australia. <sup>4</sup>Indonesian Centre for Archaeology, Jl. Raya Condet Pejaten No. 4, Jakarta 12001, Indonesia.

\*To whom correspondence should be addressed. E-mail: dfalk@fsu.edu

rived occipital expansion over the cerebellum of *H. erectus* (Fig. 1B), and its endocast is relatively wider (more brachycephalic) (Fig. 1A and fig. S3). LB1's endocast least resembles the microcephalic's (Fig. 1 and fig. S2), which has a pointed frontal lobe, compressed occipital lobe, and flattened posterior end, with the caudalmost poles on the cerebellum. Although our sample includes only one microcephalic endocast, its shape conforms to features of its corresponding skull that typify primary microcephaly (microcephalia vera): small cranial vault relative to face, sloping forehead, and pointed vertex (11, 12). The only

criterion for secondary microcephaly is an occipitofrontal circumference below  $-2$  SD for age and sex (11), but these data are unavailable for LB1's population. Unless a *H. erectus*-like endocast shape is characteristic of an unrecognized form of secondary microcephaly, we reject the hypothesis that LB1 was a pathological microcephalic (4).

Length, breadth, height, and frontal breadth measurements were collected from endocasts (Table 1 and table S1) and used to generate six ratios (Table 1). In a principal-components analysis, LB1 groups with *H. erectus* and is separate from *H. sapiens*, Sts 5 (fig. S4), and

the pygmy, based on the first principal component (weighted heavily on relative height and the disparity between maximum breadth and frontal breadth), and is separate from *H. erectus* and the microcephalic in the second principal component (weighted heavily on breadth relative to length) (Fig. 2A). LB1 bears little resemblance to the pygmy (fig. S5). Typically, pygmy skulls are over 1000 cm<sup>3</sup> (ours measures 1249 cm<sup>3</sup>) and resemble those of neighboring humans in shape (13). Unlike LB1, whose brain/body size ratio scales like that of an australopithecine, however, the ratio for pygmies is slightly larger than that found in

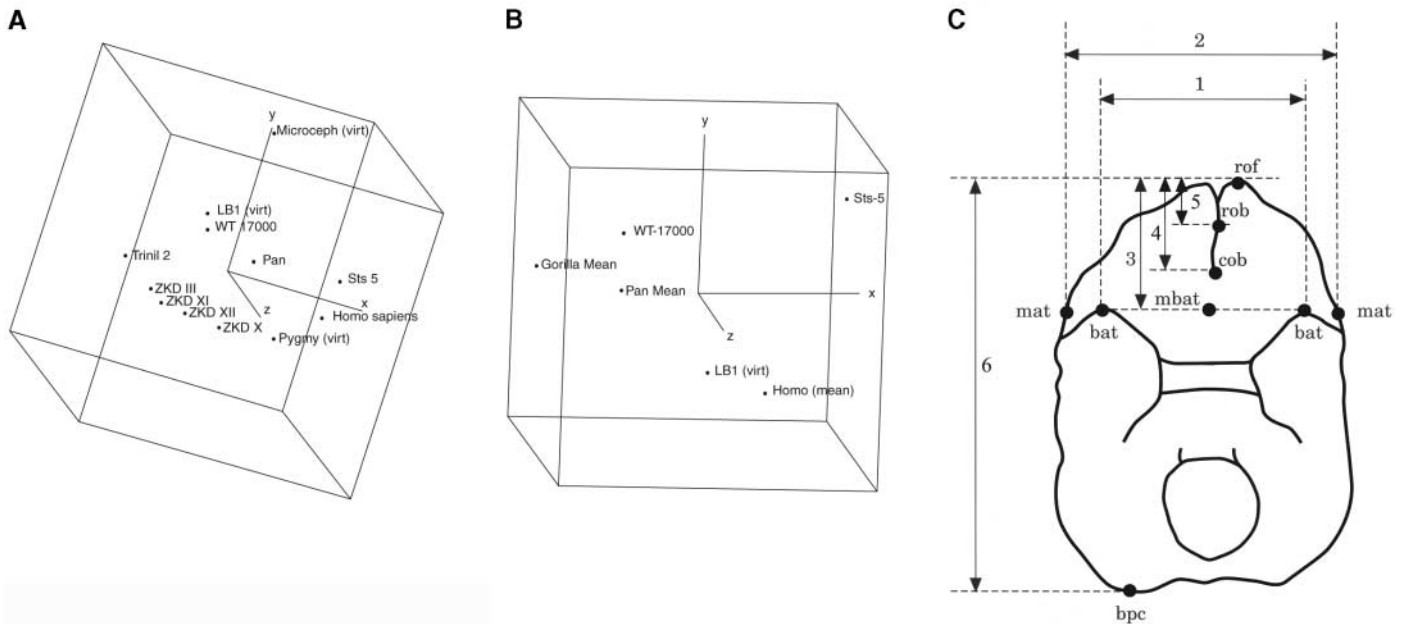


**Fig. 2.** Plots of principal components and key for basal view measurements. (A) Plots of the first three principal components resulting from the analysis of the endocast indices listed in Table 1 [excluding B-FB/H, which was highly correlated with B-FB/L ( $r = 0.98$ )]. First, second, and third principal components are aligned along the x, y, and z axes. (B) Plots of the first three principal components resulting from the analysis of basal-view endocast indices listed in table S2. (C) Key for basal view data analyzed in (B) (9). Measurements obtained from basal views were

projected onto the horizontal (basal) plane from endocasts. Landmarks: bat, most anterior point on temporal lobe from basal view; mat, most lateral point on endocast at the level of bat in basal plane; mbat, middle of the line connecting the two bats; rof, the most rostral point on the orbital surfaces of the frontal lobes; cob, caudal boundary of olfactory bulbs (cribriform plate) in the midline; rob, rostral boundary of olfactory bulbs in the midline; bcp, most posterior point on the cerebellum in basal view.

**Table 1.** Endocast measurements (in mm) of length, breadth, height, frontal breadth, and resulting indices.

	Length	Breadth	Height	Frontal breadth	Breadth/length	Height/length	Frontal breadth/length	(Breadth – frontal breadth)/length	(Breadth – frontal breadth)/height	Height/breadth
<i>Pan troglodytes</i> ( $n = 7$ )	108.8	88	75.3	72.8	0.81	0.69	0.67	0.14	0.20	0.86
<i>H. sapiens</i> ( $n = 7$ )	168.0	128.0	122.0	114.0	0.76	0.73	0.68	0.08	0.11	0.95
KNM-WT 17000*	113.4	92.9	72.5	78.1	0.82	0.64	0.69	0.13	0.20	0.78
Sts 5†	119.1	93.5	86.3	85.6	0.79	0.72	0.72	0.07	0.09	0.92
ZKD III (skull E1)‡	158.6	124.5	99.7	91.4	0.78	0.63	0.58	0.21	0.33	0.80
ZKD X (skull LI)‡	174.6	130.4	114.9	106.7	0.75	0.66	0.61	0.14	0.21	0.88
ZKD XI (skull LII)‡	165.9	127.2	103.7	97.1	0.77	0.63	0.59	0.18	0.29	0.82
ZKD XII (skull LIII)‡	167.4	128	108.5	97.8	0.76	0.65	0.58	0.18	0.28	0.85
Trinil 2§	156.7	126.9	95	92.5	0.81	0.61	0.59	0.22	0.36	0.75
Microcephalic	89.1	84.4	66.3	63.7	0.95	0.74	0.71	0.23	0.31	0.79
Pygmy	165.7	123.9	116.9	102.6	0.75	0.71	0.62	0.13	0.18	0.94
LB1	119.6	102.8	81.4	77.7	0.86	0.68	0.65	0.21	0.31	0.79

\**Paranthropus aethiopicus*. †*A. africanus*. ‡*H. erectus* (formerly *Sinanthropus*, China). §*H. erectus* (formerly *Pithecanthropus*, Java).

||Computer model, virtual endocast.

their nonpygmy neighbors, giving their heads a relatively large appearance (14). This is expected because pygmies scale allometrically along ontogenetic curves (15), leading to relatively enlarged heads and brains, as is the case for human youngsters relative to adults (16) (fig. S1). The laws governing allometric scaling of brain/body ratios are powerful and hold within other species of primates (17, 18).

For this reason, and because the morphologies of our endocast samples differ greatly, we do not believe that LB1 represents a human pygmy (19).

A second principal-components analysis was performed on measurements from the base of LB1's endocast and compared to similar measurements from 10 gorillas, 18 chimpanzees, 10 *H. sapiens*, KNM-WT 17000

(*Paranthropus aethiopicus*), and Sts 5 (9) (Fig. 2, B and C, and tables S2 and S3). The *H. erectus* endocasts were excluded because their bases were missing. The first and second principal-components analyses group LB1 exclusively with *H. sapiens* (Fig. 2B). The first principal component is most heavily weighted on 4/6 and 5/6 (Fig. 2C), which represent the relative projection of the prefrontal cortex rostral to both the anterior and posterior margins of the olfactory bulb. The second principal component is most heavily weighted on 3/6 and (6-3)/6, which represent the relative length of the frontal lobes rostral to the temporal poles and the relative length of the brain caudal to the temporal poles. As in humans, the most anterior sectors of LB1's orbital surfaces are lengthened.

The lambdoid suture is located more rostrally on the left than on the right side of the endocast (Fig. 3). Both the skull and the endocast show a left frontal and right occipital petalia (Fig. 1A) that, in humans, are statistically correlated to some degree with left-handedness (20). After entering the middle cranial fossa, small anterior branches of the middle meningeal vessels course rostrally across the ventral surface of the right temporal lobe and across the ventrolateral surface on the left. On the right, a branch from another meningeal vessel enters the middle braincase from the orbital region and courses caudally across the temporal lobe inferior to the Sylvian fissure. Similar orbital contributions are common in apes and have been reported for certain *H. erectus* endocasts by some workers (21) but not others, who used a scoring system for modern humans (22). Traces of meningeal vessels are also reproduced in the right parietal region, and several arachnoid granulations appear near the vertex on the right. LB1 reproduces somewhat (artificially) distorted transverse and sigmoid sinuses. A cast of the parietal emissary foramen appears near the medial end of the left lambdoid suture.

The right side of LB1's endocast reproduces part of the Sylvian fissure and numerous small sulci on the lateral temporal and dorsolateral frontal lobes (Fig. 3). The right orbital surface reveals three small sulci that do not extend onto the dorsal surface (the left orbital surface is damaged). In the left occipital region, LB1 reproduces an inferior occipital sulcus and a small crescent-shaped lunate sulcus medial to it and caudal to the lambdoid suture. The position of the lunate sulcus is derived and suggests cortical reorganization in the posterior parietal association cortex as compared with apes (2, 23).

LB1's orbital caps are not delimited rostrally by apelike orbitofrontal sulci that incise the borders and course toward the temporal poles on the orbital surfaces (23, 24). Instead, LB1's gyrification, orientation, and relation-

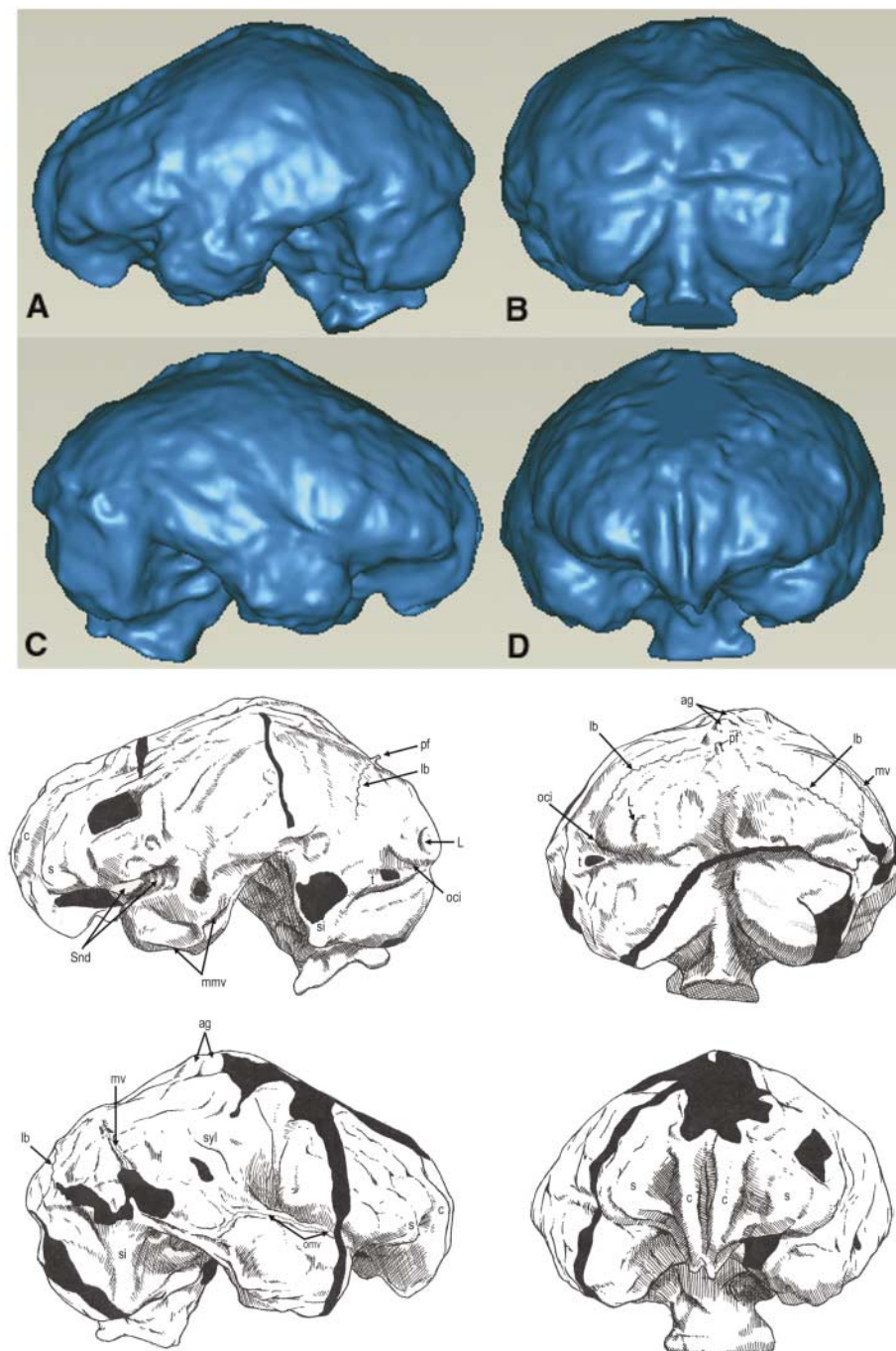


**Fig. 3.** Virtual endocast of LB1 (top). Views: (A), left lateral; (B), posterior; (C), right lateral; (D), frontal. Identifications of features are shown on corresponding sketches (bottom) (damaged areas are blackened) as follows: ag, arachnoid granulations; c, frontal lobe convolutions; lb, lambdoid suture; L, lunate sulcus; mv, meningeal vessels; mmv, middle meningeal vessels; oci, inferior occipital sulcus; omv, orbital meningeal vessels; pf, foramen for parietal emissary vein; s, frontal lobe swelling; si, sigmoid sinus; Snd, Sylvian notch and depression; Syl, Sylvian fissure; t, transverse sinus.

ship of the lateral prefrontal cortex relative to the temporal poles appear derived. Following Connolly (23), we decline to identify rami that border the human pars triangularis (part of Broca's area) on the left, although the general morphology in this region would be consistent with their existence. On the left (and to a lesser extent the right), a distinct Sylvian notch separates the temporal from the frontal lobe and continues caudally as a depression. This region corresponds to a Sylvian crest within the skull of LB1 that, in humans, sometimes occurs in particularly thick skulls and is correlated with Sylvian depressions on endocasts, although the brains are, if anything, more opercularized in the corresponding area (23).

The depression for the superior sagittal sinus on LB1's frontal lobes is bordered laterally by large convolutions [which probably contained additional furrows not reproduced on the endocast (23)] that curve around the rostral tip of the endocast onto the orbital surface and meet at the foramen caecum. Dimples separate these convolutions laterally from swellings that square off the frontal lobes and give their outline a ruffled appearance in dorsal view (Fig. 1A). Although hints of such contours may be seen in chimpanzee and hominin endocasts such as in the no. 2 specimen from Sterkfontein (9), the extent of these expansions in the frontal polar region of LB1 is unusual. This part of the prefrontal cortex in humans and apes consists of Brodmann's area 10, which in humans may be involved in higher cognitive processes such as the undertaking of initiatives and the planning of future activities (25). Human frontal lobes are not larger than expected for apes of similar brain volume (26), but area 10 is both absolutely and relatively enlarged in *H. sapiens* as compared with apes (25). LB1's polar convolutions appear derived compared with those of *H. erectus* and other early hominins. Unlike the frontal lobes, human temporal lobes appear to be somewhat larger than expected for an ape brain of human size (26–28); thus, LB1's extremely wide temporal lobes (brachycephaly; fig. S3) may represent another derived feature.

Our data show that LB1's well-convoluted brain could not have been a miniaturized version of the brain of either *H. sapiens* or *H. erectus*. Nevertheless, its similarities with *H. erectus* strongly suggest a phylogenetic connection, although its australopithecine-like brain/body size ratio and morphology of the femur and pelvis (29) are not expected in a miniaturized descendant of a larger-bodied *H. erectus* (which, instead, would be expected to scale allometrically along the ontogenetic curve predicted for *H. erectus*) (fig. S1). Although it is possible that *H. floresiensis* represented an endemic island dwarf that, over time, became subject to unusual allometric constraints, an

alternative hypothesis is that *H. erectus* and *H. floresiensis* may have shared a common ancestor that was an unknown small-bodied and small-brained hominin (1).

# References and Notes

1. P. Brown et al., *Nature* **431**, 1055 (2004).
2. R. L. Holloway, D. C. Broadfield, M. S. Yuan, *The Human Fossil Record, Volume Three, Brain Endocasts—The Paleoneurological Evidence* (Wiley-Liss, Hoboken, NJ, 2004).
3. M. J. Morwood et al., *Nature* **431**, 1087 (2004).
4. M. Henneberg, A. Thorne, *Before Farming* (online journal) **4**, article 2 (2004).
5. G. C. Conroy, M. W. Vannier, in *Hominid Evolution: Past, Present and Future*, P. V. Tobias, Ed. (Liss, New York, 1985), pp. 419–426.
6. G. C. Conroy, M. Vannier, P. V. Tobias, *Science* **247**, 838 (1990).
7. G. C. Conroy et al., *Science* **280**, 1730 (1998).
8. F. Spoor, N. Jeffery, F. Zonneveld, *J. Anat.* **197**, 61 (2000).
9. Falk et al., *J. Hum. Evol.* **38**, 695 (2000).
10. The CT-estimated cranial capacity was 417 cm<sup>3</sup>, as opposed to 380 cm<sup>3</sup> measured with mustard seeds (1). The 37-cm<sup>3</sup> difference is attributable to variation in how cranial holes were plugged and thus to measurement error associated with the current reconstructions.
11. A. Verloes, *Orphanet Encyclopedia*, www.orpha.net/data/patho/GB/uk-MVMSG.pdf (February 2004).
12. A. Kumar et al., *J. Biosci.* **27**, 629 (2002).
13. W. H. Flower, *J. Anthropol. Inst. G. B. Ireland* **18**, 3 (1889).
14. L. L. Cavalli-Sforza, in *African Pygmies*, L. L. Cavalli-Sforza, Ed. (Academic Press, New York, 1986), pp. 81–93.
15. B. T. Shea, R. C. Bailey, *Am. J. Phys. Anthropol.* **100**, 311 (1996).
16. R. Passingham, *New Scientist* **27**, 510 (1975).
17. A. H. Schultz, *Primates* **1**, 887 (1956).
18. H. Jerison, *Evolution of the Brain and Intelligence* (Academic Press, New York, 1973).
19. J. Diamond, *Science* **306**, 2047 (2004).

20. M. LeMay, *Am. J. Neuroradiol.* **13**, 493 (1992).
21. D. Falk, *Am. J. Phys. Anthropol.* **92**, 81 (1993).
22. F. Weidenreich, *Palaentol. Sinica New Ser. D*, **3**, 1 (1938).
23. C. J. Connolly, *External Morphology of the Primate Brain* (Thomas, Springfield, IL, 1950).
24. D. Falk, *Science* **221**, 1072 (1983).
25. K. Semendeferi et al., *Am. J. Phys. Anthropol.* **114**, 224 (2001).
26. K. Semendeferi, in *Evolutionary Anatomy of the Primate Cerebral Cortex*, D. Falk, K. R. Gibson, Eds. (Cambridge Univ. Press, Cambridge, 2001), pp. 257–289.
27. K. Semendeferi, H. Damasio, *J. Hum. Evol.* **38**, 317 (2000).
28. J. K. Rilling, R. A. Seligman, *J. Hum. Evol.* **42**, 505 (2002).
29. C. Groves, *Before Farming* (online journal) **4**, article 1 (2004).
30. We thank the National Geographic Society (grant 7760-04) and D. Hamlin for helping to bring this research to fruition. X. Wu of the Institute of Vertebrate Paleontology and Paleoanthropology, Chinese Academy of Sciences, provided the measurements for *H. sapiens* in Table 1; K. Mowbray of the American Museum of Natural History provided the cast of the microcephalic skull and pygmy skull; and B. Latimer and L. Jellema of the Cleveland Museum of Natural History loaned additional skeletal material. We appreciate T. Gebke and C. Tinscher's technical assistance in CT scanning, B. Macy's production of physical endocasts, B. Worthington's illustrations of LB1's endocast (Fig. 3), and E. Chambless's help with manuscript preparation.

# Supporting Online Material

www.sciencemag.org/cgi/content/full/1109727/DC1

Materials and Methods

SOM Text

Figs. S1 to S5

Tables S1 to S3

References

13 January 2005; accepted 11 February 2005

Published online 3 March 2005;

10.1126/science.1109727

Include this information when citing this paper.

## Vasopressin and Oxytocin Excite Distinct Neuronal Populations in the Central Amygdala

Daniel Huber,<sup>1</sup> Pierre Veinante,<sup>2</sup> Ron Stoop<sup>1\*</sup>

Vasopressin and oxytocin strongly modulate autonomic fear responses, through mechanisms that are still unclear. We describe how these neuropeptides excite distinct neuronal populations in the central amygdala, which provides the major output of the amygdaloid complex to the autonomic nervous system. We identified these two neuronal populations as part of an inhibitory network, through which vasopressin and oxytocin modulate the integration of excitatory information from the basolateral amygdala and cerebral cortex in opposite manners. Through this network, the expression and endogenous activation of vasopressin and oxytocin receptors may regulate the autonomic expression of fear.

The amygdala plays an important role in anxiety and fear behavior. Fear learning involves its lateral and basolateral parts, where

the association between incoming fearful and neutral stimuli leads to potentiation of synaptic transmission. These parts project to the central amygdala (CeA), whose efferents to the hypothalamus and brainstem trigger the autonomic expression of fear (1). Selective gating of synaptic transmission through the CeA could therefore modulate the fear response (2, 3). Indeed, recent studies suggest that increased inhibition within the CeA could underlie the anxiolytic effects of benzodiazepine-

<sup>1</sup>Department of Cellular Biology and Morphology and Centre for Psychiatric Neuroscience, Department of Psychiatry, Centre Hospitalier Universitaire Vaudois, University of Lausanne, Switzerland. <sup>2</sup>Neurophysiologie Cellulaire et Intégrée, Unité Mixte de Recherche 7519, CNRS, Université Louis Pasteur, Strasbourg, France.

\*To whom correspondence should be addressed. E-mail: rstoop@unil.ch